Network Structure in GeS2−Sb2S3 Chalcogenide Glasses: Raman Spectroscopy and Phase Transformation Study

ARTICLE *in* THE JOURNAL OF PHYSICAL CHEMISTRY C · FEBRUARY 2012

Impact Factor: 4.77 · DOI: 10.1021/jp208614j

8 AUTHORS, INCLUDING:

Changgui Lin
Ningbo University
85 PUBLICATIONS **585** CITATIONS
SEE PROFILE

Yinsheng Xu
Ningbo University
56 PUBLICATIONS **453** CITATIONS
SEE PROFILE

Tiefeng Xu
Ningbo University
183 PUBLICATIONS **1,157** CITATIONS
SEE PROFILE

Qiuhua Nie
Ningbo University
242 PUBLICATIONS **1,208** CITATIONS
SEE PROFILE

THE JOURNAL OF PHYSICAL CHEMISTRY C

Article

pubs.acs.org/JPCC

Network Structure in GeS_2–Sb_2S_3 Chalcogenide Glasses: Raman Spectroscopy and Phase Transformation Study

Changgui Lin,*[,†,‡] Zhuobin Li,[‡] Lei Ying,[‡] Yinsheng Xu,[†,‡] Peiqing Zhang,[‡] Shixun Dai,*[,‡] Tiefeng Xu,[‡] and Qiuhua Nie[‡]

[†]The School of Materials Science & Chemical Engineering, Ningbo Univeristy, Ningbo 315211, Zhejiang, People's Republic of China

[‡]Laboratory of Infrared Materials and Devices, Ningbo University, Ningbo 315211, Zhejiang, People's Republic of China

ABSTRACT: Structural order beyond the next-nearest-neighbor structural units is of great interest in network glasses, especially in chalcogenide glasses, but little specific description can be reached. Here, the structure of pseudobinary $(100 - x)GeS_2$–xSb_2S_3 chalcogenide glasses is elucidated using differential scanning calorimetry, Raman scattering, and laser-induced phase transformation experiments over its full range $(0 \leq x \leq 100)$ of compositions. We observe two compositional thresholds of $x = 40$ and 50 in the calorimetric experiments, which are confirmed by Raman scattering and laser-induced phase transformation studies, respectively. Three structural features can be derived from these results: the structural motifs in this glass network are the $[SbS_3]$ pyramid and $[GeS_4]$ tetrahedra, respectively; at $x \geq 40$, the connection between $[GeS_4]$ tetrahedra vanishes; and at $x \geq 50$, the aggregation of four $[SbS_3]$ units happens, preparing for the laser-induced crystallization of Sb_2S_3 crystallites. Combined with valuable indication from the topological thresholds, a specific structural model covering the arrangement of structural units in a large atomic scale is clarified, which can perfectly explain all the experimental results. This work provides a new way to get insight into the intermediate-range order of glass networks and understand their related physical properties.

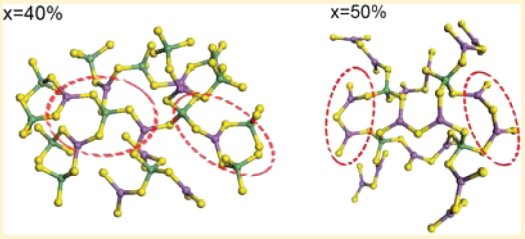

1. INTRODUCTION

The nature of glassy networks continues to be one of the central issues in glass science that is necessary for understanding basic network properties, such as their behavior under optical irradiation or extremes of pressure and temperature, and materials with new functional properties are to be designed. Nevertheless, structural ordering in network glasses (especially covalently bonded glasses) on medium-range length scales has long been a source of controversy.[1−3] Detailed experimental information is necessary to understand both the network properties and the fundamentals of glass formation. As typical covalently bonded amorphous solids, the intermediate-range order in chalcogenide glasses has attracted considerable interest.[4−10] In the past decades, a majority of studies were devoted to realize the building blocks (structural motif) of the network structure in chalcogenide glass (structural units, such as $[GeS_4]$ tetrahedra,[11,12] $[SbS_3]$ pyramid,[13−15] and ethane-like $[S_3Ga\text{-}GaS_3]$[16,17]). Recently, new insights into the so-called Boolchand intermediate phase have been discovered in chalcogenide glasses from the point of view of chemical bonds by two parameters: glass formation ability and average electronegativity.[18] Starting with compositional trends in glass transition behavior, the nanoscale phase separation, network demixing, or self-organization was evidenced to be existing in binary or ternary chalcogenide glasses, combined with the experimental results of mechanical properties and Raman scattering, etc.[18] The knowledge of the microstructure in chalcogenide glasses has been further improved. However, the description of the local glassy network is still ambiguous. No specific structural order of the structural motifs was clarified beyond the next-nearest-neighbor ones.

Generally speaking, a precise description of a glassy structure over a wide range of length scales is notoriously difficult to obtain because the atomic arrangement is not an ordered lattice. Since the pioneering work of Zachariasen,[19] fortunately, modeling of network glasses has been regarded as a useful approach to explicitly address the problem of describing topological and chemical ordering in structurally disordered glass systems. Numerous studies have been focused on specific structural models in some binary glasses of Ge–X, Si–X, and As–X (X = S or Se) systems.[2,5,6,20−22] However, that of ternary chalcogenide glasses was scarcely depicted due to the extremely complicated situation when one more element joins in. Detailed experimental information is necessary to describe the microscopic connectivity of their structural motifs.

This study here demonstrates an attempt to describe a specific arrangement of structural motifs with a large atomic scale (medium-range order, MRO) in GeS_2–Sb_2S_3 glasses, which are especially selected for the following two reasons. First, their microstructure is one of the most active and attractive topics concerning how the connectivity of three-coordinated $[SbS_3]$ and four-coordinated $[GeS_4]$ units contribute to the large glass-forming region[23] and flexible thermal and optical properties.[13,24−27] Second, the structural

Received: September 7, 2011
Revised: February 3, 2012
Published: February 9, 2012

motifs in GeS_2−Sb_2S_3 glasses are simple enough to expediently construct their intermediate-range order. Different from the existence of metal−metal bonds in GeS_2−M_2S_3 (M = Ga or In) glasses, only [SbS_3] and [GeS_4] structural units are included in this case.[13,28−31] Despite that the said structural motifs have been established firmly, it is generally believed that the challenges to understanding glass structures by the local probes of structures alone (vibrational spectroscopy and diffraction methods) are enormous and have met with limited success. Thus, hereinafter, systematical experiments are carried out to obtain abundant structural features for achieving a specific description of the connectivity of structural motifs in GeS_2−Sb_2S_3 chalcogenide glasses. We investigated the inelastic (Raman scattering) and thermal (glass transition and phase transformation behavior) response of the studied glasses examined as a function of glass compositions. Three compositional windows of glass transition were characterized by differential scanning calorimetry (DSC), indicating the existence of different glass phases in the intermediate structural range. With the help of Raman spectrometry, structural motifs were well-studied and phase transformation behavior was also revealed by laser-induced experiments. The thresholds of thermal behavior were found, manifesting the evolution of the network structure (specified here as the three-dimensional network structure of chalcogenide glasses). Combined with the above experimental results, we illustrated the MRO microstructure in the GeS_2−Sb_2S_3 glass system.

2. EXPERIMENTAL SECTION

Glasses with stoichiometric compositions of $(100 - x)GeS_2$−xSb_2S_3 (in mol %) were prepared by the melt-quenching technique, where x ranges from 0 to 90 (designated as xSb), respectively. Batches (10 g) of highly pure raw materials (Ge, Sb, and S of 99.999%) were weighed and placed into silica ampules, which were then sealed under vacuum (~10^{-3} Pa). The ampule with an inner diameter of 9 mm was placed into a rocking furnace, heated to 960 °C, and maintained for 12 h, then homogenized at 880 °C for 1.5 h, and finally quenched in ice water. Subsequently, the obtained glass sample was annealed below the glass transition temperature (T_g −10 °C) for 3 h to minimize inner constraints and finally slowly cooled to room temperature. The glass disks of 1.2 mm in thickness were obtained from the glass rod and polished to optical quality on both sides. Details of the glass preparation can also be found elsewhere.[32] Glassy Sb_2S_3 (designated as 100Sb) was obtained by thermal evaporation on a silica substrate. Sb_2S_3 crystallite (c-Sb_2S_3) confirmed by the X-ray diffraction (XRD) technique was obtained by slowly cooling the stoichiometry Sb_2S_3 melt under vacuum (~10^{-3} Pa). The compositions of the prepared glasses were analyzed by electron probing microanalysis (EPMA, type: JXA-8800R), revealing that the difference between theoretical and real composition was within a reasonable range (±1 atom %).

The calorimetric measurements were carried out using DSC (type: TA Q2000) with a temperature accuracy of ±1 °C. The characteristic temperatures of glass, such as the glass transition temperature (T_g) and the temperature of onset crystallization (T_x), were obtained by heating an ~10 mg sample in a hermetic aluminum pan at a 10 °C/min rate under a N_2 atmosphere. DSC runs usually are not completed until the crystallization peak finishes, but the highest heating temperature is limited to <600 °C to avoid melting the aluminum pan. Meanwhile, to avoid the contamination of the DSC furnace by the evaporation of glass samples, the maximum temperature is also limited by T_g + 200 °C or the liquidus temperature. Raman scattering spectroscopy was conducted at room temperature using the back (180°) scattering configuration by a laser confocal Raman spectrometer (type: Renishaw inVia) using an Ar ion laser with a wavelength of 488 nm. Under the same configuration, the CW laser was also used as an irradiation source, which was focused onto samples using a 50× (NA = 0.75) microscope objective (Leica). Different laser powers of 2.5 and 0.05 mW were specified to induce and characterize the phase transformation behavior of these samples, respectively. For Raman spectroscopy, a grating with 1800 grooves/mm was used in this spectrometer.

3. RESULTS AND DISCUSSION

3.1. Glass Structure Characterization. To investigate structural motifs in the glass network, we conducted Raman scattering measurements with polarization modes. Polarized Raman spectra of the $(100 - x)GeS_2$−xSb_2S_3 system ($0 \le x \le 100$) are shown in Figure 1a,b. HH and HV represent the parallel and perpendicular configuration of the incident and scattering light, respectively. The ratio of the HV/HH intensities is called the depolarization ratio (ρ). It provides structural information on the symmetry of the vibrational modes. The inset of Figure 1a shows that the intensity of HV spectra of GeS_2 glass is about 7 times less than that of HH spectra. Strong polarization dependences are observed in GeS_2 glass, so do the other samples. Four major peaks are observed at 290, 340, 370, and 432 cm^{-1}. In Figure 1a,b, the intensity increases for the 300 cm^{-1} peak, but decreases for peaks at 340, 370, and 432 cm^{-1} as the Sb_2S_3 content increases. According to the literature,[33,34] the Raman bands of 340 and 370 cm^{-1} are ascribed to the A_1 and A_1^c modes of [GeS_4] tetrahedra, respectively, and the 432 cm^{-1} peak is related to the vibration of edge-shared [GeS_4] tetrahedra. As indicated in Figure 1, the ascription of the 340 cm^{-1} feature is further supported by its depolarization ratio, in which a strong depolarization of $\rho \approx 0.13$ is shown for the A_1 symmetry. On the contrary, the asymmetric stretching mode is responsible for the Raman features of 370 and 432 cm^{-1}. For the Raman peak at 290 cm^{-1}, its intensity increases with the addition of Sb_2S_3 content. In the data present in Figure 1, we observed a combination of two peaks that formed the Raman peak at 290 cm^{-1}. Therefore, a peak-fitting program based on the Gaussian profile was employed to separate these two peaks. The peak positions derived from deconvolution are around 280 and 308 cm^{-1}, respectively. The bands at 280 and 308 cm^{-1} are also the main vibrational modes for c-Sb_2S_3 crystallites, as shown in Figure 1. It is well known that Sb atoms are solely linked with S in the structural configuration of c-Sb_2S_3.[35] Thus, it is believed that [SbS_3] pyramidal vibrations are responsible for these two Raman peaks at 280 and 308 cm^{-1}, other than for a sole broad band at 290[28,29,31] or 300 cm^{-1}.[13,30] Furthermore, a strong depolarization is also observed for the Raman band at 308 cm^{-1}, suggesting that it is related to the asymmetric stretching mode of [SbS_3] pyramidal. The Raman band at 280 cm^{-1} is originated from the A_1 symmetric stretching vibration of [SbS_3] pyramidal. In a word, all the GeS_2−Sb_2S_3 glasses are composed of the fundamental units of [SbS_3] pyramids and [GeS_4] tetrahedra.

Structural information obtained above by Raman data has been restricted within the identification of structural motifs. No specific structural order beyond the next-nearest-neighbor units

dx.doi.org/10.1021/jp208614j | J. Phys. Chem. C 2012, 116, 5862−5867

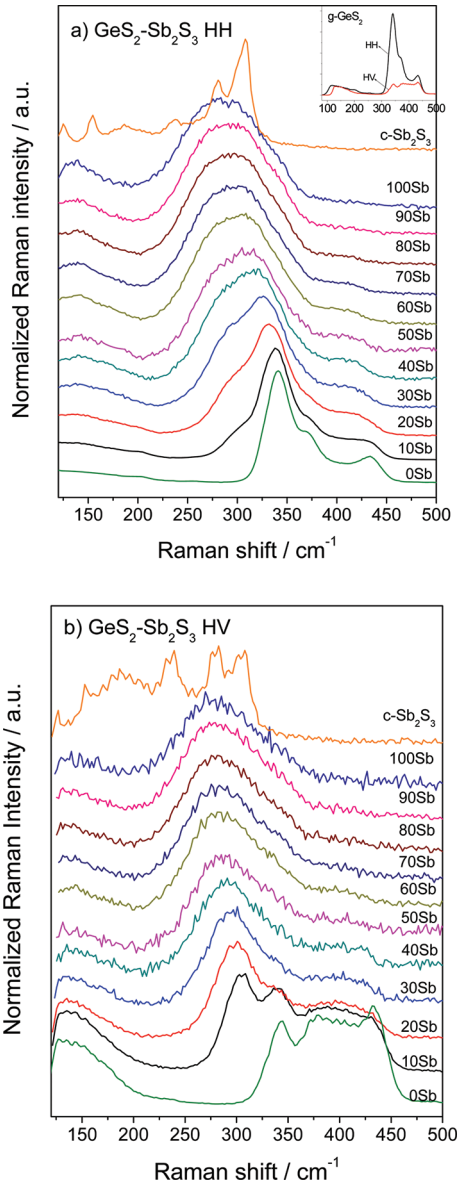

Figure 1. (a) HH and (b) HV polarized Raman spectra of GeS_2−Sb_2S_3 glasses with compositional dependences and *c*-Sb_2S_3 crystallites, respectively. The inset of (a) presents the HH and HV polarized Raman spectra of GeS_2 (0Sb) glass.

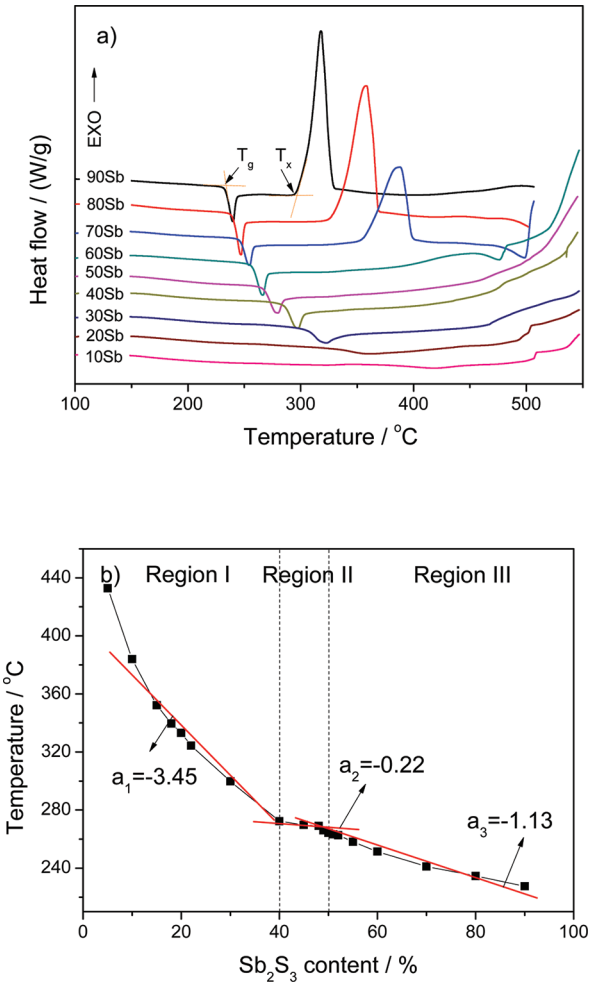

Figure 2. (a) DSC curves for the GeS_2−Sb_2S_3 glasses at a heating rate of 10 °C/min. The definition of T_g is also shown. (b) Compositional trend of T_g in GeS_2−Sb_2S_3 glasses plotted as a function of Sb_2S_3 content (x mol %). The red lines are the guides to eye.

can be clarified. Other approaches are essential to understanding the glass network of MRO scale. In recent years, Boolchand et al.[36−38] have presented that glass forming compositions, and, particularly, the composition variation of T_g in chalcogenide glasses, contain vital clues on the connectivity of the network framework. Figure 2a shows the DSC curves of GeS_2−Sb_2S_3 glass samples. Although most of the crystallization peaks are absent, it is seen that the compositional tendency of T_x and $\Delta T(=T_x - T_g)$ is roughly similar with the previous work.[13] The compositional trend of T_g defined in Figure 2a is plotted as a function of Sb_2S_3 content, x, as displayed in Figure 2b. It is obvious that the T_g decreases with increasing x. For the glass networks possessing identical connectivity, T_g usually scales with the bond strength of the network linkage. The Ge−S bond strength (55.5 kcal/mol) highly exceeds that of Sb−S bonds (48.8 kcal/mol),[39] which is responsible for the decreasing trend of T_g in the studied samples. A perusal of the data of Figure 2b also shows that the T_g does not linearly vary with the increase of Sb_2S_3 content, suggesting that there is different connectivity in the glass network.[36−38] The slope dT_g/dx is largest in the $0 < x < 40$ range (designated as Region I), then is lowest in a narrow range of $40 \leq x \leq 50$ (Region II), and increases slightly in the higher Sb_2S_3 content of $x > 50$ (Region III). Threshold behavior in T_g is observed in the quasi-binary GeS_2−Sb_2S_3 glasses, near $x = 40$ and 50, respectively. We, therefore, take it as evidence for network demixing in this stoichiometric glass system.[36−38]

To further examine the threshold behavior, laser-induced changes in GeS_2−Sb_2S_3 glasses were investigated particularly under the Raman spectrometer configuration. A high excitation power of ~2.5 mW was selected to conduct possible structural modification. The Raman spectra with low- and high-intensity irradiation were collected in Figure 3, yielding threshold information of their phase transformation behavior. It is clear that phase transformation behavior changes within the compositions of 40−60 mol % Sb_2S_3 content. Raman spectra of these original glasses are similar with a feature of a broad band located at 290 cm^{-1}, as shown by the solid lines in Figure 3. Of greater interest is to see a clear change of phase transformation behavior of these glass samples after high-power laser irradiation (see the dashed lines in Figure 3). At $50 \leq x \leq$

dx.doi.org/10.1021/jp208614j | J. Phys. Chem. C 2012, 116, 5862−5867

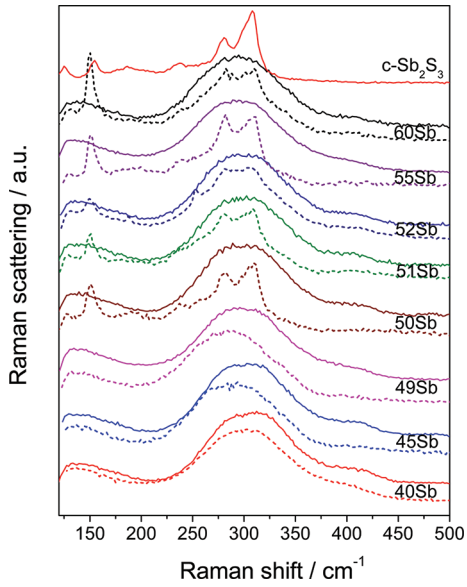

Figure 3. Raman scattering spectra for characterization of the laser-induced changes in GeS_2−Sb_2S_3 glasses after laser irradiation with different powers of 0.05 and 2.5 mW, respectively. The solid lines represent the samples after laser irradiation with a power of 0.05 mW, whereas the dashed lines are for those after the irradiation of 2.5 mW power.

60, Raman scattering peaks located at 150, 280, and 308 cm^{-1} appear, whereas no observable ones grow in the glass samples of $x < 50$. By comparison with the Raman spectrum of standard Sb_2S_3 crystals confirmed by XRD pattern (not shown here), it is evidenced that Sb_2S_3 crystals are laser-induced in the glasses with compositions of $50 \leq x \leq 60$. We assign the slight shift of the broad Raman band to modification of glass phases for the glass samples of $x < 50$. Apparently, the threshold of phase transformation behavior is at $x = 50$. It is worthy to note that distinct from phase transition by heat treatment, the laser-induced change does not have a strong connection with the thermal stability ($\Delta T = T_x - T_g$). Its mechanism is still unclear and needs to be further investigated. These data of threshold behavior in T_g and laser-induced phase transformation would provoke other insights into the molecular structure of the present glasses, as we shall illustrate in the following.

3.2. Modeling of Glass Structure. To begin with, we focus on the structural implications of the T_g behavior and Raman scattering spectra near $x = 40$. As discussed above, the structural motifs of $[SbS_3]$ pyramids and $[GeS_4]$ tetrahedra build the glass network of GeS_2−Sb_2S_3 glasses. For the glass samples with low Sb_2S_3 content, it is reasonable that the $[SbS_3]$ pyramids should disperse uniformly among a large number of $[GeS_4]$ tetrahedra, as shown in Figure 4a. The Sb_2S_3 additive increases the number of $[SbS_3]$ pyramids. It then raises issues about what the glass network would be when the $[SbS_3]$ pyramids increase just enough to be isolated by these $[GeS_4]$ tetrahedra. Which composition is responsible for the topological threshold? The topological threshold is, therefore, described as follows: the three-coordinated $[SbS_3]$ pyramid is isolated by three $[GeS_4]$ tetrahedral units, and the four-coordinated $[GeS_4]$ tetrahedra are separated by four $[SbS_3]$ pyramidal units. That is, the ratio of $[GeS_4]$ to $[SbS_3]$ units is 3:4. As indicated in Figure 4b, the compositional threshold of this model is at $x = 40$. It is in excellent agreement with the threshold behavior in T_g, as shown in Figure 2b, which is a solid

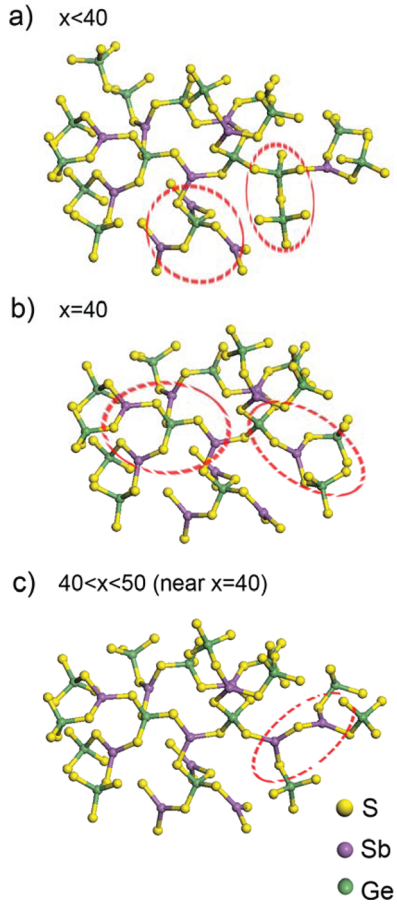

Figure 4. Schematic representation showing the MRO structure of glasses with compositions of (a) $x < 40$, (b) $x = 40$, and (c) $40 < x < 50$ (near $x = 40$).

evidence for this structural model. We can see that, as displayed in Figure 4c, the aggregation of $[SbS_3]$ units, that is, the $[S_2$-Sb-S-Sb-$S_2]$ unit, would happen once the Sb_2S_3 content exceeds 40% ($x > 40$). Consequently, the structural model of the glass network near $x = 40$ has been constructed by understanding the thermal data of T_g behavior. Additionally, perusal of Figure 4 gives us another clue that the $[GeS_4]$ tetrahedra are isolated when $x \geq 40$. No Raman features for the corner- or edge-shared $[GeS_4]$ tetrahedra, as marked by red circles in Figure 4a, should be observed for the glass samples in Region II. Noteworthy in Raman scattering spectra is the variation of Raman bands at 432 and 370 cm^{-1} now, which are ascribed to the vibration of edge-shared $[GeS_4]$ tetrahedra. As shown in Figure 5, the intensity of the Raman band at 432 cm^{-1} decreases with the increasing content of Sb_2S_3 and disappears for the samples of $x \geq 40$. The vanishing of the Raman band at 432 cm^{-1} suggests that no linkage between the $[GeS_4]$ tetrahedra is existing, as depicted in Figure 4b,c. Consequently, further confirmation for the structural model in Figure 4 is given by Raman scattering spectra.

Let us dissect the indications of structural fluctuations from the topological threshold near $x = 50$, which locates between Region II and Region III, as shown in Figure 2b. There is firm evidence that the glass structure changes in the proximity of $x = 50$, leading to the radical variation of laser-induced phase transformation behavior, as indicated in Figure 3. From the point of the precipitation of Sb_2S_3 crystals, the structural

dx.doi.org/10.1021/jp208614j | J. Phys. Chem. C 2012, 116, 5862−5867

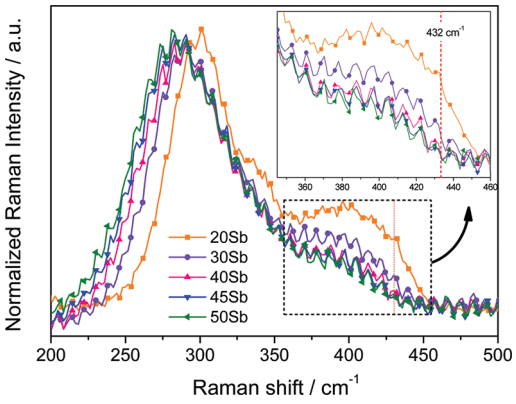

Figure 5. HV polarized Raman spectra of GeS_2−Sb_2S_3 glasses with compositions of x = 20, 30, 40, 45, and 50.

configuration of Sb and S atoms should be essentially ready for crystallographic organization in the glass network of the studied samples. It has been found that the repeating unit building the crystal of antimony trisulfide is Sb_4S_6, and its correct chemical formula is $(Sb_4S_6)_\infty$.[35] Consequently, it is acceptable to assume that no Sb_2S_3 crystals would be precipitated if the number of nearest-neighbor structural units of $[SbS_3]$ is forced down into four in the local structural arrangement of GeS_2−Sb_2S_3 glasses. Taking the four-coordinated $[S_2$-Sb-S-Sb-$S_2]$ unit as unity, as shown in Figure 6a, four $[GeS_4]$ tetrahedra are necessary to segregate it, and so do that for the four-coordinated $[GeS_4]$ tetrahedra. The ratio of $[S_2$-Sb-S-Sb-$S_2]$ to $[GeS_4]$ units should be 1:1 (x = 50) for this topological threshold. According to the above assumption, when the ratio of $[S_2$-Sb-S-Sb-$S_2]$ to $[GeS_4]$ units is more than 1:1 (x > 50), two or more $[S_2$-Sb-S-Sb-$S_2]$ units should be connected as marked by the red circle in Figure 6b. It provides the basis of the structural configuration for the separation of Sb_2S_3 crystals during the laser-induced experiments. In the case of glass samples of 40 < x < 50 (Region II), the decrease of Sb_2S_3 content leads to detachment of the $[S_2$-Sb-S-Sb-$S_2]$ units to $[SbS_3]$ pyramids, as marked by the red circles in Figure 6c. This structural model is verified reciprocally by comparison with that in Figure 4c. So far, structure implications of these experimental results have been extracted as the structure model shown in Figures 4 and 6.

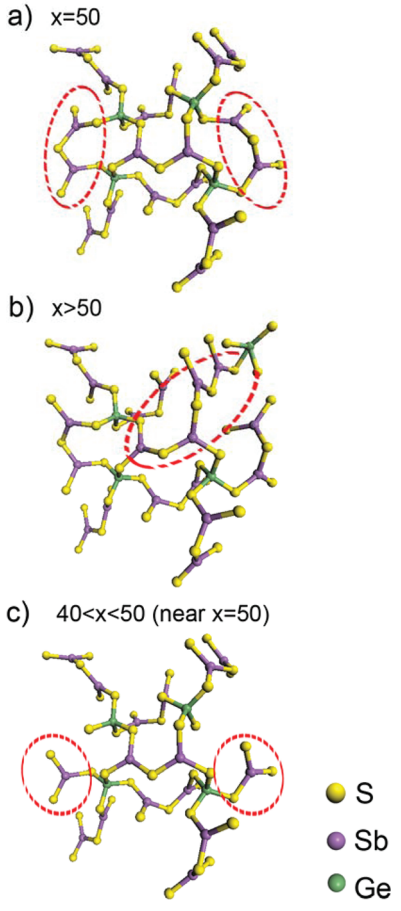

Figure 6. Schematic representation showing the MRO structure of glasses with compositions of (a) x = 50, (b) x > 50, and (c) 40 < x < 50 (near x = 50).

3.3. Microscopic Origin of the Physical Properties.

With the knowledge of the structural model for this glass system, as shown in Figures 4 and 6, it would be pertinent here to discuss the microscopic origin of the T_g behavior in Figure 2b. There is growing recognition that compositional dependence of T_g behavior is an excellent indication for global connectivity of the glass network. In this study, these results permit one to establish that, besides the main decreasing trend of T_g determined by bond strengths, with the addition of Sb_2S_3, different global connectivity of the glass network apparently affects its behavior in the following ways. First, the three-coordinated $[SbS_3]$ pyramids that appear in the network at 0 < x < 40 strongly loosen the rigidity of the glass structure constructed by four-coordinated $[GeS_4]$ tetrahedra. It results in a large decrease in T_g for the glass samples in Region I, as shown in Figure 2b. At 40 ≤ x < 50, the emergence of a new glass phase of the $[S_2$-Sb-S-Sb-$S_2]$ unit leads to a flat profile of T_g variation, making a compositional threshold at x = 40. As indicated in Figures 4c and 6c, these four-coordinated nanophases grow in concentration at the expense of the $[SbS_3]$ units, maintaining the rigidity of the intermediate-range order of glasses with compositions of 40 ≤ x < 50. Thus, T_g of the glasses in Region II keeps steady. Finally, the aggregation of $[S_2$-Sb-S-Sb-$S_2]$ nanophases at x ≥ 50, as displayed in Figure 6a, is responsible for the further decease of T_g. The slope dT_g/dx decreases slightly compared with that in Region I. It can be ascribed to that the structural motif formed with the increasing Sb_2S_3 content is the $[S_2$-Sb-S-Sb-$S_2]$ unit now, other than the $[SbS_3]$ pyramid. We thus arrive at the notion that the microscopic origin for these experimental data is elucidated in detail.

4. CONCLUSIONS

Structural motifs of the $[SbS_3]$ pyramid and $[GeS_4]$ tetrahedra in $(100 - x)GeS_2$−xSb_2S_3 glasses are identified by employing HH and HV polarized Raman scattering measurement. Compositional trends in T_g further provide valuable insights into the molecular structure of the studied glasses. The compositional thresholds in the T_g behavior are located at x = 40 and 50, which are confirmed by Raman scattering and laser-induced phase transformation studies, respectively. With a perusal of these experimental results, a novel glass network model extending to intermediate-range order is specifically depicted. At x = 0, the network structure consists of $[GeS_4]$ tetrahedra in a stochastic manner. As x increases to 40, the Sb_2S_3 additive alloys as $[SbS_3]$ in the $[GeS_4]$ backbone with no connection between these $[SbS_3]$ units provided by the separation of $[GeS_4]$. These three-coordinated $[SbS_3]$ units

dx.doi.org/10.1021/jp208614j | J. Phys. Chem. C 2012, 116, 5862−5867

strongly lower the global connectedness of the backbone, as reflected in T_g values. At $x = 40$, the $[SbS_3]$ pyramids are well isolated by $[GeS_4]$ tetrahedra reciprocally. In the $40 < x \leq 50$ range, the additive continues to alloy as $[SbS_3]$ in the $[GeS_4]$ backbone, but this time with the formation of $[S_2\text{-Sb-S-Sb-}S_2]$ units due to the excess $[SbS_3]$ for the finite $[GeS_4]$. The generation of this new glass phase slows down the decreasing trend in T_g and leads to another threshold of $x = 50$. When the addition of Sb_2S_3 reaches $x = 50$, all $[SbS_3]$ units are present in the form of four-coordinated $[S_2\text{-Sb-S-Sb-}S_2]$, which are also isolated by $[GeS_4]$ tetrahedra reciprocally. At still higher x (>50), the structural motifs of $[S_2\text{-Sb-S-Sb-}S_2]$ are aggregated as a self-organized structural phase leading to the laser-induced crystallization of Sb_2S_3. Consequently, the specific medium-range structure of $GeS_2-Sb_2S_3$ chalcogenide glasses is realized and contributes to understanding their physicochemical properties.

AUTHOR INFORMATION

Corresponding Author

*E-mail: linchanggui@nbu.edu.cn (C.L.), daishixun@nbu.edu.cn (S.D.).

Notes

The authors declare no competing financial interest.

ACKNOWLEDGMENTS

This work was partially supported by the Program for Innovative Research Team of Ningbo City (Grant No. 2009B21007), the Natural Science Foundation of Ningbo City (Grant No. 2011A610091), the Zhejiang Provincial Natural Science Foundation of China (Grant Nos. R1101263 and Y4110322), the Program for New Century Excellent Talents in University (Grant No. NCET-10-0976), and the National Natural Science Foundation of China (Grant Nos. 61108057, 61177087, and 60978058). It was also sponsored by K.C. Wong Magna Fund in Ningbo University.

REFERENCES

(1) Salmon, P. S.; Martin, R. A.; Mason, P. E.; Cuello, G. J. *Nature* **2005**, *435*, 75−78.
(2) Elliott, S. R. *Nature* **1991**, *354*, 445−452.
(3) Stillinger, F. H. *Science* **1995**, *267*, 1935−1939.
(4) Tverjanovich, A.; Tveryanovich, Y. S.; Loheider, S. *J. Non-Cryst. Solids* **1996**, *208*, 49−55.
(5) Takebe, H.; Maeda, H.; Morinaga, K. *J. Non-Cryst. Solids* **2001**, *291*, 14−24.
(6) Boolchand, P.; Georgiev, D. G.; Goodman, B. *J. Optoelectron. Adv. Mater.* **2001**, *3*, 703−720.
(7) Cuisset, A.; Hindle, F.; Laureyns, J.; Bychkov, E. *J. Raman Spectrosc.* **2010**, *41*, 1050−1058.
(8) Boolchand, P.; Jin, M.; Novita, D. I.; Chakravarty, S. *J. Raman Spectrosc.* **2007**, *38*, 660−672.
(9) Lin, C.; Calvez, L.; Tao, H.; Allix, M.; Moréac, A.; Zhang, X.; Zhao, X. *J. Solid State Chem.* **2011**, *184*, 584−588.
(10) Musgraves, J. D.; Carlie, N.; Hu, J.; Petit, L.; Agarwal, A.; Kimerling, L. C.; Richardson, K. A. *Acta Mater.* **2011**, *59*, 5032−5039.
(11) Lucovsky, G.; Galeener, F. L.; Keezer, R. C.; Geils, R. H.; Six, H. A. *Phys. Rev. B* **1974**, *10*, 5134.
(12) Zhao, X.; Higuchi, H.; Kawamoto, Y. *Phys. Chem. Glasses* **1998**, *39*, 98−100.
(13) Takebe, H.; Hirakawa, T.; Ichiki, T.; Morinaga, K. *J. Ceram. Soc. Jpn.* **2003**, *11*, 572−575.
(14) Cervinka, L.; Hruby, A. *J. Non-Cryst. Solids* **1982**, *48*, 231−264.
(15) Cervinka, L.; Smotlacha, O.; Tichý, L. *J. Non-Cryst. Solids* **1987**, *97−98*, 183−186.
(16) Julien, S. B. C.; Massot, M.; Chbani, N.; Cai, X.; Loireau-Lozac'h, A. M.; Guittard, M. *Mater. Sci. Eng., B* **1994**, *22*, 191−200.
(17) Ivanova, Z. G. *J. Mol. Struct.* **1991**, *245*, 335−340.
(18) Popescu, M., Velea, A., Eds. *Rigidity and Boolchand Intermediate Phases in Nanomaterials*; Optoelectronic Materials and Devices; INOE: Bucharest, Romania, 2009; Vol. *6*, pp 413−433.
(19) Zachariasen, W. H. *J. Am. Chem. Soc.* **1932**, *54*, 3841−3851.
(20) Yang, G.; Bureau, B.; Rouxel, T.; Gueguen, Y.; Gulbiten, O.; Roiland, C.; Soignard, E.; Yarger, J. L.; Troles, J.; Sangleboeuf, J.-C.; Lucas, P. *Phys. Rev. B* **2010**, *82*, 195206.
(21) Boolchand, P.; Chen, P.; Vempati, U. *J. Non-Cryst. Solids* **2009**, *355*, 1773−1785.
(22) Sugai, S. *Phys. Rev. B* **1987**, *35*, 1345.
(23) Tichá, H.; Tichý, L.; Rysavá, N.; Tríska, A. *J. Non-Cryst. Solids* **1985**, *74*, 37−46.
(24) Svadlák, D.; Zmrhalová, Z.; Pustková, P.; Málek, J.; Pérez-Maqueda, L. A.; Criado, J. M. *J. Non-Cryst. Solids* **2008**, *354*, 3354−3361.
(25) Málek, J.; Zmrhalová, Z.; Barták, J.; Honcová, P. *Thermochim. Acta* **2010**, *511*, 67−73.
(26) Shiryaev, V. S.; Troles, J.; Houizot, P.; Ketkova, L. A.; Churbanov, M. F.; Adam, J. L.; Sibirkin, A. A. *Opt. Mater.* **2009**, *32*, 362−367.
(27) Shánelová, J.; Kostál, P.; Málek, J. *J. Non-Cryst. Solids* **2006**, *352*, 3952−3955.
(28) Frumarová, B.; Bílková, M.; Frumar, M.; Repka, M.; Jedelský, J. *J. Non-Cryst. Solids* **2003**, *326−327*, 348−352.
(29) Ichikawa, M.; Wakasugi, T.; Kadono, K. *J. Non-Cryst. Solids* **2010**, *356*, 2235−2240.
(30) Petit, L.; Carlie, N.; Adamietz, F.; Couzi, M.; Rodriguez, V.; Richardson, K. C. *Mater. Chem. Phys.* **2006**, *97*, 64−70.
(31) Shtets, P. P.; Fedelesh, V. I.; Kabatsij, V. M.; Malesh, V. I.; Shpak, I. I.; Gorvat, A. A. *J. Optoelectron. Adv. Mater.* **2001**, *3*, 937−940.
(32) Lin, C.; Calvez, L.; Rozé, M.; Tao, H.; Zhang, X.; Zhao, X. *Appl. Phys. A* **2009**, *97*, 713−720.
(33) Lin, C.; Tao, H.; Zhu, W.; Wang, B.; Zang, H.; Zheng, X.; Zhao, X. *J. Non-Cryst. Solids* **2009**, *355*, 438−440.
(34) Lucovsky, G.; deNeufville, J. P.; Galeener, F. L. *Phys. Rev. B* **1974**, *9*, 1591−1597.
(35) Popescu, M. A. *Non-Crystalline Chalcogenides*; Kluwer Academic Publishers: New York, 2000.
(36) Mitkova, M.; Wang, Y.; Boolchand, P. *Phys. Rev. Lett.* **1999**, *83*, 3848.
(37) Chen, P.; Holbrook, C.; Boolchand, P.; Georgiev, D. G.; Jackson, K. A.; Micoulaut, M. *Phys. Rev. B* **2008**, *78*, 224208.
(38) Boolchand, P.; Georgiev, D. G.; Qu, T.; Wang, F.; Cai, L.; Chakravarty, S. *C. R. Chim.* **2002**, *5*, 713−724.
(39) Nikolic, P. M.; Vujatovic, S. S.; Todorovic, D. M. *J. Phys. C: Solid State Phys.* **1986**, *19*, L717.